LEAN PREMIXED COMBUSTION/ACTIVE CONTROL - 1998

Topical Reports

D. J. Seery

DOE Contract No. DE-AC22-95PC95144

Research Center

1998

LEAN PREMIXED COMBUSTION/ACTIVE CONTROL

SUMMARY

An experimental comparison between two contrasting fuel-air swirlers for industrial gas turbine applications was undertaken at the United Technologies Research Center. The first, termed an Aerodynamic nozzle, relied on the prevailing aerodynamic forces to stabilize the downstream combustion zone. The second configuration relied on a conventional bluff plate for combustion stability and was hence named a Bluff-Body nozzle. Performance mapping over the power curve revealed the acoustic superiority of the Bluff-Body nozzle. Two dimensional Rayleigh indices calculated from CCD images identified larger acoustic driving zones associated with the Aerodynamic nozzle relative to its bluff counterpart. The Bluff-Body's success is due to increased flame stabilization (superior anchoring ability) which reduced flame motion and thermal/acoustic coupling.

INTRODUCTION

Reduction in NO_x/CO emissions while maintaining acoustic stability over all engine power levels is essential to the viability and durability of any gas turbine to be used for large-scale industrial applications. Continued reductions in EPA emission levels and the need to operate in low emissions mode over the engine operating range continue to drive lean-premixed combustion systems toward their lean stability limits.

Lean-premixed combustion systems are designed to maintain constant flame temperature as the engine changes power levels in an effort to control emissions over the operating range. Operation over the power curve has been described elsewhere Ref. 1)-Ref. 4). In all cases, stability of the lean-premixed combustion system relies upon the ability of the premixing fuel injector to maintain stable combustion while it is subjected to changes in the governing variables: nozzle equivalence ratio and inlet air temperature and pressure. Coupled to such experimental works are numerical efforts designed to model system acoustics/stability in simplistic, yet rigorous forms Ref. 5)-Ref. 7).

This paper examines the ability of two fuel-air mixing swirler designs to minimize combustion induced pressure oscillations. These configurations which were based on earlier tangential entry (TE) nozzles Ref. 8), Ref. 9), were evaluated as part of a larger study of fuel-air mixing swirlers being considered for industrial applications. Parameters investigated included the use of premixed and diffusion flame pilots, variations in combustor exit Mach number, aerodynamic versus bluff-body stabilization, equivalence ratio, and inlet pressure and temperature. As the designs exhibited different flame stabilization mechanisms, they, in turn, exhibited contrasting dynamics (combustor acoustics). Identification of the optimal fuel-air swirler design for the combustion system was the focus of the present work.

EXPERIMENTAL SET-UP

The implementation of acoustically quiet fuel nozzle designs into the lean combustion system was planned in three stages: (1) single nozzle rig tests to screen designs for acoustic performance while maintaining low emissions operation similar to or better than prior art; (2) sector rig tests to confirm acoustic and emissions performance demonstrated in the single nozzle rig and to map part power operation; (3) full engine tests to develop and optimize combustor performance. The acoustic results obtained during the first phase are the focus of the present paper.

Fuel Nozzle Designs

Figure 1a details an earlier aerodynamic nozzle design Ref. 8) whose center-body was modified for the present investigation as discussed elsewhere Ref. 9) (see Fig. 1b). A diffusion pilot was added to the tip of the center-body for configuration 1 (upper sketch, Fig. 1b) to evaluate the acoustic sensitivity with piloting. Inherent with the addition of a diffusion pilot is poor NO_x emissions performance. To evaluate the tradeoffs between a diffusion pilot and a premixing pilot, a second design modification was made (lower sketch). For this configuration, 7% of the total airflow and fuel were taken from the two inlet scrolls and premixed inside the center-body using a swirler of identical swirl as the main flow. The end of the center-body was also recessed to enhance mixing between the scroll and center-body flows while the end cap was extended into the scroll inlets to maintain similar interior velocities and main fuel penetration characteristics of configuration 1.

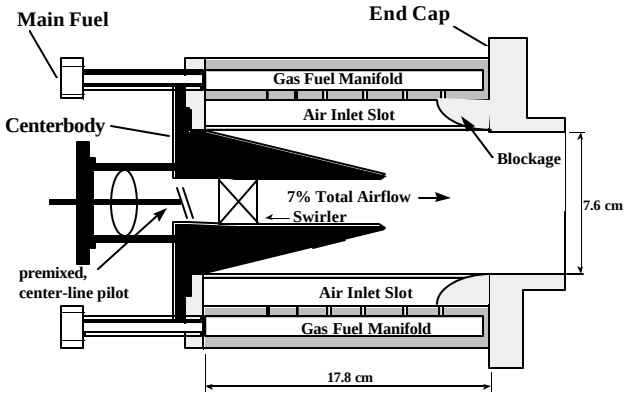

Figure 1a. Schematic of an earlier Aerodynamic Nozzle

The premixed and diffusion pilot designs provided opposing boundary conditions to the central recirculation zone located downstream. The diffusion pilot design relied upon a bluff-body for flame stability while the premixed pilot had an aerodynamically stabilized flame (open end, interior swirler). As such, the diffusion pilot and premixed pilot designs will be referred to as a Bluff-Body nozzle and Aerodynamic nozzle, respectively. Both have an effective nozzle flow area of approximately 26.2 cm^2 and similar center-body contouring.

Single Nozzle Rig

The single nozzle rig (SNR) shown in Fig. 2, facilitated independent control of the air and gas fuel (natural gas) flows and inlet temperature and pressure supplied to the premixing fuel nozzle. Airflow was metered using a choked, main air venturi and heated using a non-vitiated, indirect gas fired heater. Fuel flow rates were similarly metered using choked venturis. A perforated plate located upstream of the fuel nozzle, provided a uniform feed of air to the nozzle to simulate the air supply volume of the engine. The fuel nozzle was mounted on a bulkhead which allowed approximately 55% of the total airflow to pass through the nozzle and the remainder to act as bypass air Ref. 9).

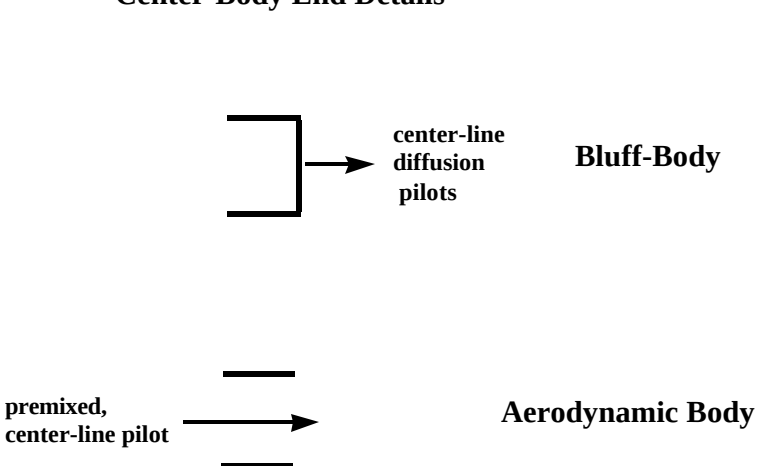

Figure 1b. Schematic of the Center-Body End Details

Forty-two percent of this bypass air, in turn, fed small diameter cooling holes while fifty-eight percent feed four dilution holes on the combustor liner. The axi-symmetric liner simulated the engine combustor volume and aspect ratio and incorporated a side-wall, diffusion pilot. Fluctuating pressure measurements were made inside the plenum (P_3) and combustor (P_4) using infinite tube probes (ITP). Emission measurements were also made using an array of water-cooled probes inserted into another plate. A T-Section downstream of this plate diverted the flow to allow for optical access (PMT and video camera). Combustor liner pressure drop was controlled using a back-pressure valve downstream of the T-section. Typical operating conditions are detailed in Table 1.

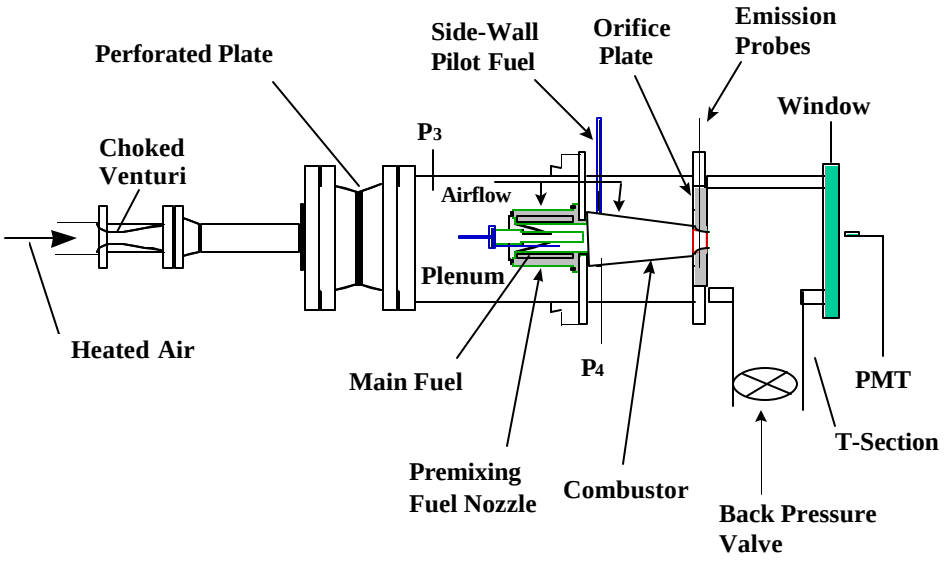

Figure 2. Schematic of the Single Nozzle Rig

The equivalence ratio ("Front End Equivalence Ratio" or f_{fe} in the table) is defined as all the fuel divided by the nozzle airflow only. The overall equivalence ratio, therefore, is simply the flow split (0.55) times f_{fe}. Piloting levels are percentages of the total fuel flow rate. For the range of operating pressures examined, the mass flow rate of air was between 2.3 and 4.5 Kg/s.

Table 1
Operating Conditions

Operating Pressure (P_3)	10.2-19.0 atm.
Inlet Temperature (T_3)	620-706 K
Equivalence Ratio (f_{fe})	0.57-0.77
Side-Wall Pilots (%SW)	5%
Diffusion Center-Line Pilots (%CL)	0-5%
Premixed Center-Line Pilots (%CL)	11-20%

The above range of equivalence ratios defined operating conditions whereby the observed pressure oscillations were controlled by the excitation of system acoustic modes (bulk/Helmholtz or axial) Ref. 9). The results presented herein focus on results at an operating pressure of 15.6 atm.

Chemiluminescence Measurements

Two dimensional chemiluminescence measurements were achieved through use of a Stanford Model 4 Quick 05 CCD video-camera connected to a fiber optic bundle (Ref. 10). This bundle was inserted into a port within the combustor liner approximately 2.5 *cm* downstream of the nozzle's exit plane. A 430 *nm* narrow band pass filter was inserted in front of the camera to isolate chemiluminescence from excited CH/CO_2 radicals existing within the flame (Ref. 11). To coordinate the image acquisition with the acoustic cycle, the camera was phased-locked with the combustor's dynamic pressure trace. Images taken at the same phase angle over roughly 112 acoustic cycles were averaged to reduce signal noise. Eight images per cycle were recorded.

THEORETICAL DEVELOPMENT: RAYLEIGH'S CRITERION

Any investigation of unstable combustion cannot be achieved without addressing the chemical-acoustic interactions that inevitably occur. As shown by others (Ref. 12 - 15), it is this interaction between the pressure and the heat-release which typically sustains the instabilities. Quantification of this coupling is achieved through use of the Rayleigh Index which can be represented mathematically as:

$$R = \frac{g - 1}{g\,\bar{p}} \int_V dV \int_t^{t+t} p'(\vec{x},t)\, q'(\vec{x},t) dt \qquad (1)$$

where p' and q' are the fluctuating components of pressure and heat release, respectively, and g, t, $\bar{p}$, and V are the ratio of specific heats, cycle period, mean pressure and system volume.

The above index can be broken down into temporally or spatially varying indices by dropping the integration in either time or space, respectively. Integration over both variables, therefore, yields a Global Rayleigh Index which characterizes the overall level of acoustic coupling. This index will be shown to be an important tool in characterizing the success of a prospective nozzle.

RESULTS

Acoustic Comparison Between the Bluff-Body and Aerodynamic Nozzles

Figures 3 and 4 compare the combustor's non-dimensional rms acoustic levels for a variety of center-line piloting percentages for the aerodynamic and bluff designs, respectively. Results were at a plenum pressure of 15.6 atm., 5% side-wall piloting and Mach 0.75 exit (This denotes the exit Mach number immediately downstream of the liner).

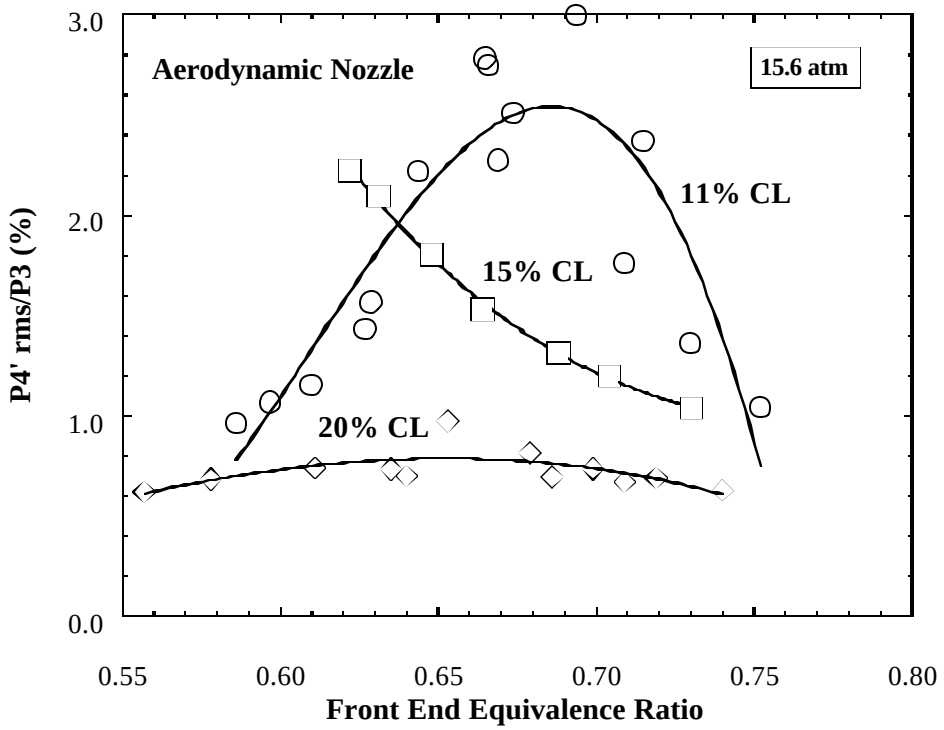

Figure 3: Acoustic Performance of the Aerodynamic Nozzle for Various Levels of Center-Line Piloting

The figures show that both nozzles behaved similarly with changes in center-line piloting (%CL): increasing %CL reduced acoustic/stoichiometric sensitivity and fluctuating combustor pressure levels (Ref. 9). For the ranges of center-line piloting shown, a factor of 4 reduction was observed for both designs. It is difficult, however, to make a direct nozzle to nozzle comparison due to the contrasting methods of piloting (diffusion versus premixed) which may obscure the separate effects of the levels of center-line piloting and roll of the bluff plate. This will, in turn, alter the overall level of premixing (fraction of premixed fuel issuing from the nozzle exit plane) and consequently emissions. A first order comparison can be made by comparing the nozzles based on identical NO_x-CO performance. This yields the following three comparisons as detailed in Table 2:

Table 2
Comparisons for Equivalent NOx/CO

Nozzle	Comparison 1	Comparison 2	Comparison 3
Bluff	0% CL	2% CL	5%CL
Aero.	11% CL	15% CL	20% CL

Using such an approach reaffirms the superiority of the bluff design. A more rigorous comparison can be made by simultaneously matching emission performance and level of premixing (Ref. 9). Since the aerodynamic nozzle implements a 95% premixing level irrespective of %CL (5% diffusion side-wall pilot used throughout), the 0% CL bluff-body configuration should be compared with the 11% CL aerodynamic run (Comparison 1). Again the superiority of the bluff design is evident. It is interesting to see how the performance of the aerodynamic design "approaches" that of its bluff counterpart at the expense of excessive piloting levels. The premixing pilot, it seems, is less effective in quelling acoustics since over 11% is needed to even approach the acoustic levels of the 0% CL bluff-body configuration.

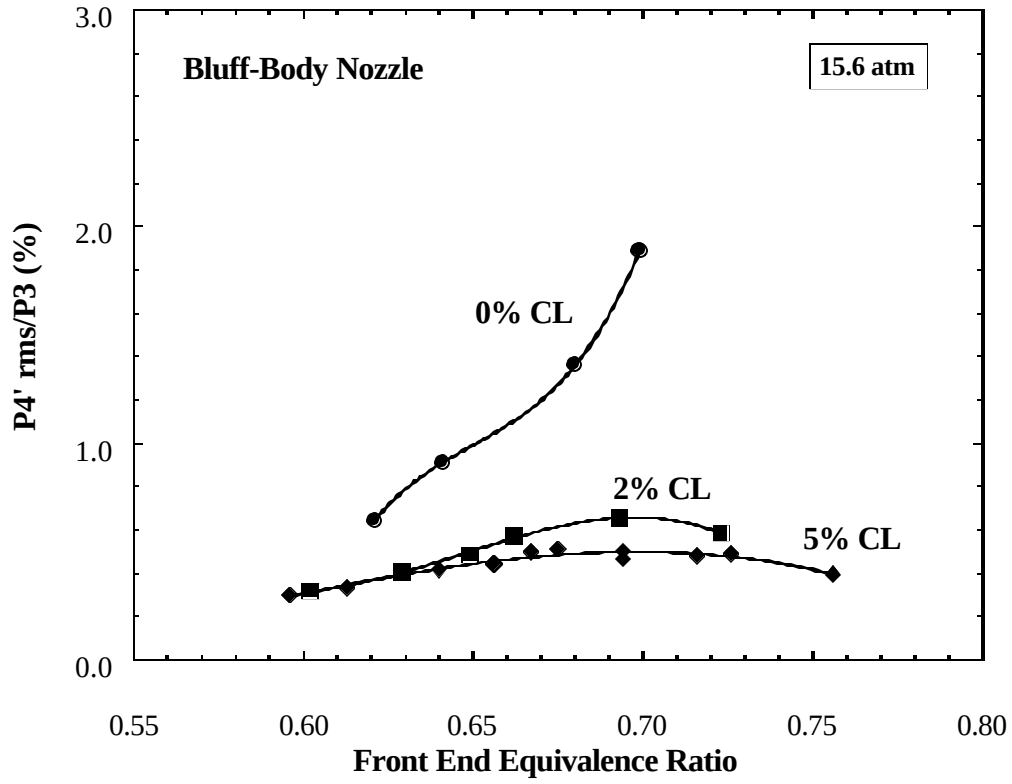

Figure 4. Acoustic Performance of the Bluff-Body Nozzle for various levels of Center-Line Piloting

A strong 220 Hz mode dominates both configurations. (Sound speed changes through fuel/air ratio adjustments will affect the exact value). Figure 5 details the corresponding power spectral

density (PSD) of the combustor's dynamic pressure trace for the Bluff-Body nozzle at 15.6 atm. and front end stoichiometry of 0.73. Analysis have shown that the observed mode emanates from a Helmholtz or bulk mode instability and is not associated with longitudinal modes present in the system (Ref. 9 and Ref. 16). These additional modes do appear with changes in the operating point but are typically weaker in magnitude.

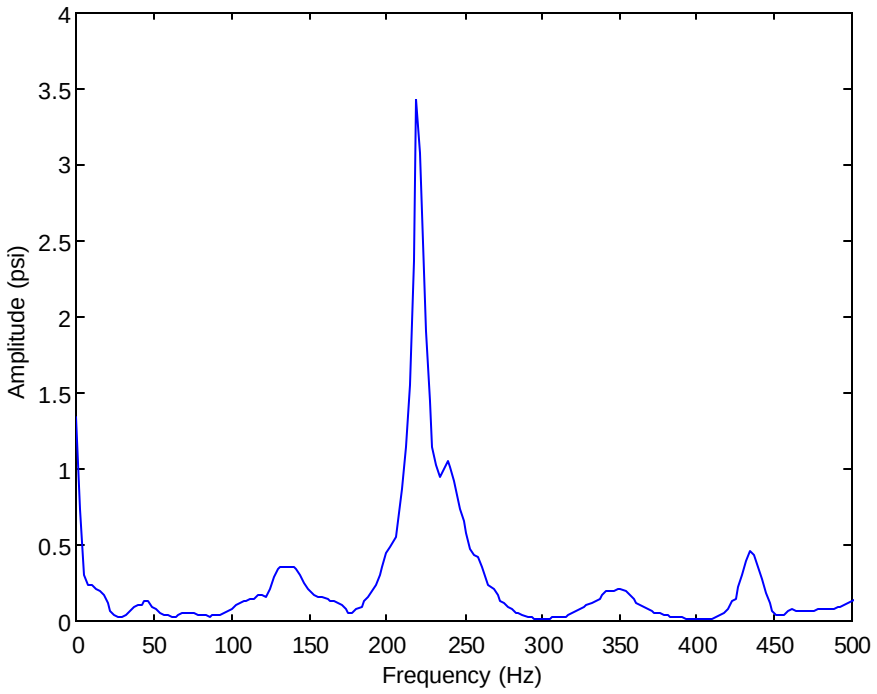

Figure 5. Power Spectral Density of Combustor Pressure for the Bluff-Body Nozzle

Figure 6 is an effort to condense the acoustic/heat release coupling mechanisms. The operating pressure was set to 15.6 atm. and the front end equivalence ratio was 0.73. Center-line piloting was 2% for the bluff design and 15% for the aerodynamic (Comparison 2, Table 2). It shows the total instantaneous heat release rate for both nozzles with respect to a generic acoustic cycle (heavy dashed line) appropriately phased. The CCD images were converted to heat release rates through the assumed linearity between chemiluminescence and heat release rate which has been proven for a fixed stoichiometry (Ref. 17 and Ref. 18). Each heat release point is simply the summation of the entire CCD array for the particular acoustic phasing. As the images were acquired through phase locking to the acoustic cycle, each point represents an average of approximately 112 acoustic cycles so the figure should reveal an accurate testament of the combustion activity occurring through the cycle. The acoustic cycle was also temporally shifted to compensate for the use of infinite tube acoustic sensors which introduce a phase delay (Ref. 19).

Clearly evident is the greater breadth through which the heat release adds energy to the acoustic cycle for the Aerodynamic nozzle. Also apparent is the more favorable phasing that the Aerodynamic nozzle's heat pulse exhibits relative to the acoustic cycle. The much weaker and less sinusoidal heat pulse fluctuations of the bluff design add less energy during the first half of the cycle and still less during the second half. The observation of increased pressure amplitudes for the Aerodynamic nozzle should now seem consistent.

The following sections will compare the designs through identification of their respective two-dimensional driving/damping zones.

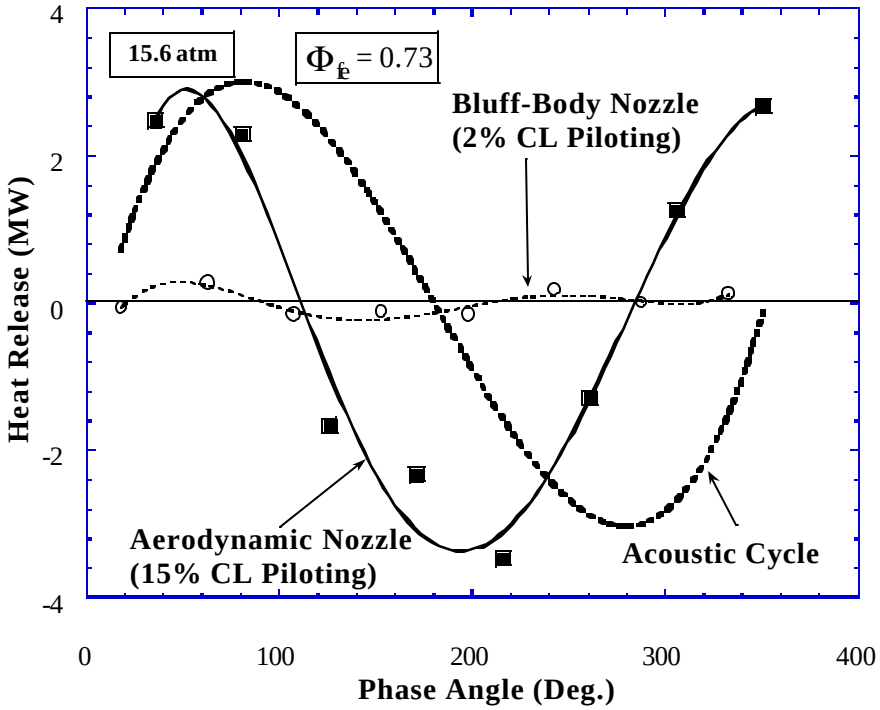

Figure 6. Acoustic/Heat Release Coupling for both Nozzles

Identification of Driving Damping Zones

The importance of the Rayleigh term in dictating how much energy can be potentially exchanged with the acoustic field is easily demonstrated by comparing with other energy addition/subtraction terms. It can be shown that the total change in acoustic energy can be expressed as (Ref. 15 and Ref. 20):

$$\frac{D}{Dt}\left(\frac{p'^2}{2g\,\bar{p}}+\frac{\bar{r}\,u'^2}{2}\right)=\frac{g-1}{g}p'q'-\frac{u'p'}{g\,\bar{p}}\frac{\partial\bar{p}}{\partial x}-\frac{\partial}{\partial x}(u'p')- \left(r'\,u'\bar{u}+\bar{r}\,u'^2+\frac{p'^2}{\bar{p}}\right)\frac{\partial\bar{u}}{\partial x} \tag{2}$$

where any flowfield variable (pressure, p, velocity, u, density, ρ, heat release, q, etc.) can be expressed as the sum of an average and a fluctuating quantity:

$$p(pressure) = \overline{p} + p' \tag{3}$$

The left hand side of (2) represent the total change in acoustic energy while the right hand side reflects how this change can occur. The first term on the right side is the previously mentioned Rayleigh term while the second and third terms are typically ignored due to the assumed orthogonality between the oscillating components of pressure and velocity. The remaining term is the mean flow gradient term which can approach appreciable values through area changes and/or in the vicinity of the combustion zone (Ref. 15). Other sources of energy addition/dissipation include contributions to the mean flow gradient, non-ideal end reflections, dissipation in the boundary layers but all pale in magnitude relative to the Rayleigh term.

Using Equation (1) and dropping the integrations in space and time, one can calculate the two-dimensional Rayleigh indices. Such images yield valuable information on the location of the driving/damping zones (Ref. 14). Figures 7 and 8 are the results for the Aerodynamic and Bluff-Body nozzles, respectively (Identical operating conditions as in Figure 6). As the figures represent instantaneous indices, the units for the contours are in $Watts/cm^2$. Black contours reflect driving zones while gray contours are damping zones. For Figure 7, the contours are equally spaced by 200 $Watts/cm^2$, while for Figure 8, they are spaced by 20 $Watts/cm^2$. Acoustic phasing is noted on each image. In the calculation, the pressure was taken to be constant spatially due to the compactness of the burning zone relative to the acoustic wavelength and the relatively small transverse direction (Ref. 14 and Ref. 21). Each instantaneous CCD image is first subtracted pixel by pixel from the averaged image and then multiplied by the oscillatory component of pressure. The process was then continued over the acoustic cycle. Although only eight "images" were recorded per cycle, each image is actually an average of around 112 cycles so the results should yield a good representation of the heat release/acoustic coupling. The only drawback of this technique is the assumption that the flowfield is two-dimensional whereas in reality it is more axisymmetric. This artifact will augment chemiluminescence measurements along the outer edge of the flow where the optical path length is longer than towards the middle of the image where it is shorter. As a consequence, the levels of driving/damping will be somewhat in error but will *not* be effected in shape or location. This latter point is more pertinent.

Clearly, regions of driving/damping are changing continuously and exhibit much two dimensionality and/or irregularity. The double peaked nature of the Aerodynamic nozzle's images (alternating driving/damping between the first two and fifth and sixth images) reflects the existence of strong stable pulsations and results when both expansion and compression waves are in phase with the minimum and maximum of the energy release profiles (Ref. 22). This characteristic, however, is not shared by its bluff counterpart. Only the second image in Figure 8 reveals strong acoustic driving of the instability. The absence of any contours in the fourth and eight images of Figure 7 indicates no driving and damping occurs at this time.

Temporally integrating each nozzle's sequence of Rayleigh images yields the net effect of driving/damping the system for a typical cycle. Results for both the Aerodynamic and Bluff-Body nozzles appear in Figures 9 and 10, respectively.

A quick examination of the images reveals the two dimensional Rayleigh Indices vary somewhat between nozzles but are characterized by alternating driving/damping regions. The above pattern can be explained by first assuming the pressure to be represented as (Ref. 14):

$$p(t) = P\cos(2\pi w\, t) \tag{4}$$

where w is the frequency of oscillation. Furthermore, the heat release may be modeled as a convecting pulse, moving, on average, at the dump plane speed u and having wavelength λ (Ref. 14 and Ref. 20):

$$q'(x,t) = Q\cos\left(2\pi (x-ut)/\lambda\right) \tag{5}$$

Hence the Rayleigh Index would read as follows:

$$R(x) = \frac{\gamma - 1}{\gamma}\int p'q'\,dt = \frac{\gamma - 1}{\gamma}PQ\cos(2\pi\, w\, x/\lambda) \tag{6}$$

where:

$$\lambda = u/w \tag{7}$$

Indeed the Rayleigh Index should adopt a sinusoidal pattern.

Comparing the aerodynamic and bluff-body images, one sees a clear spatial increase in the location of the driving zone with respect to the Bluff-Body nozzle (For the Aerodynamic nozzle, the contours are equally spaced in units of 0.5 *Joules/cm*^{2}, while for the Bluff nozzle, the corresponding units are 0.025 *Joules/cm*^{2}). The driving zone is also shifted further upstream, most likely due to the acoustic velocity fluctuations at the dump plane which evidently have a more pronounced effect on the reaction zone located downstream. In addition, the driving zone appears double peaked and also engulfs a region of damping. The more violent flow pulsations afforded by the absence of the bluff plate for the Aerodynamic nozzle have rendered the combustion zone more susceptible to acoustic driving; the flowfield has some control over the location of combustion and apparently tailors it for maximum driving.

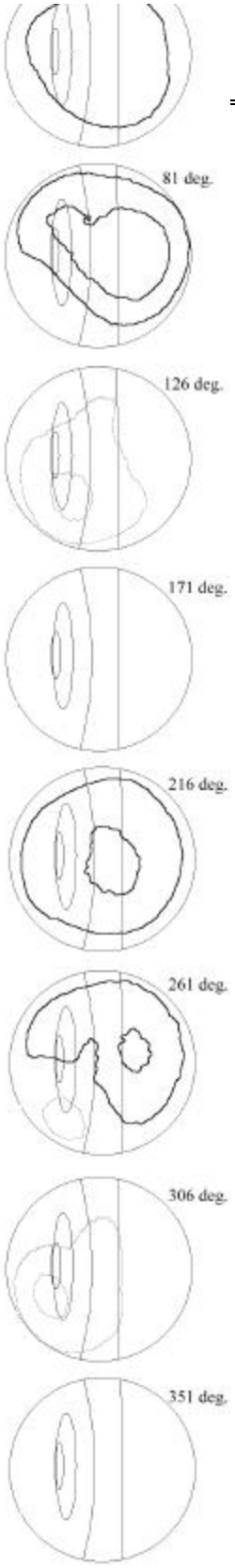

Figure 7. Instantaneous, Two-Dimensional Rayleigh Indices for the Aerodynamic Nozzle (Contours are equally spaced at *200W/cm^2*. Black are driving, gray are damping)

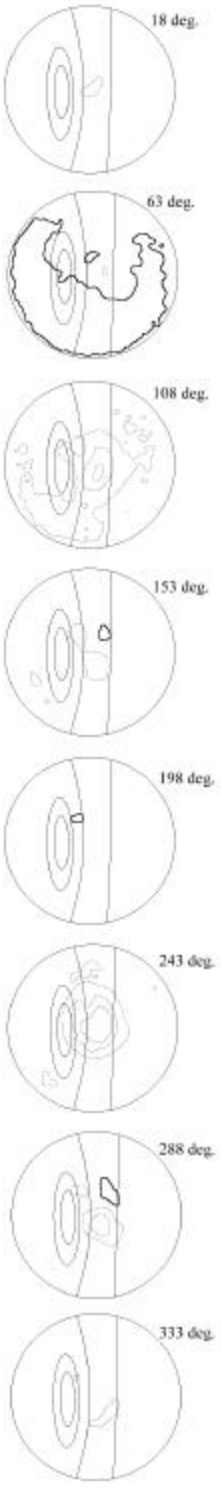

Figure 8. Instantaneous, Two-Dimensional Rayleigh Indices for the Bluff-Body Nozzle (Contours are equally spaced at *20W/cm^2*. Black are driving, gray are damping)

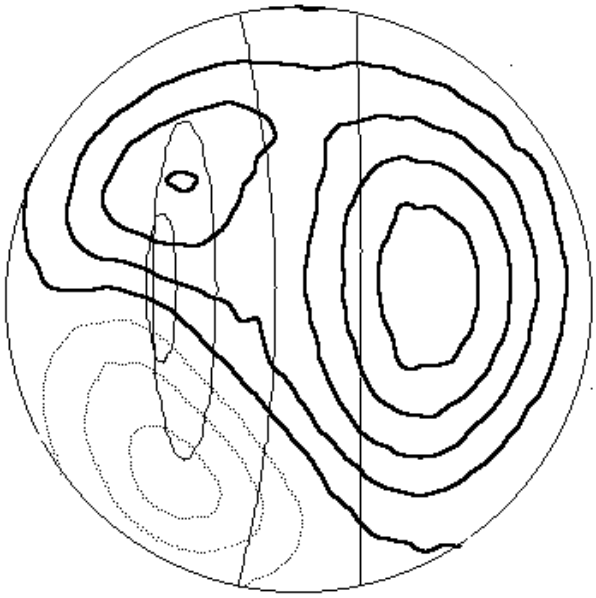

Figure 9. Global, Two-Dimensional Rayleigh Index for the Aerodynamci Nozzle

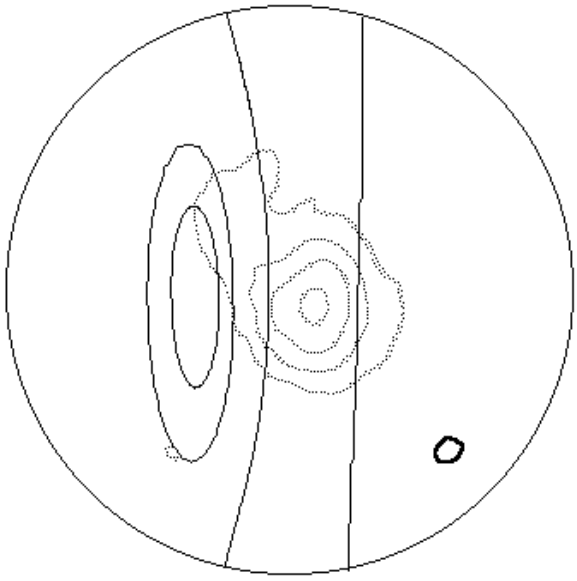

(Contours are equally spaced at 0.5J/cm^2. Black are driving, gray are damping)

Figure 10. Global, Two-Dimensional Rayleigh Index for the Bluff-Body Nozzle (Contours are equally spaced at 0.025J/cm^2. Black are driving, gray are damping)

Examination of the Bluff Body's image shows the field is dominated by a more pronounced damping zone with a small driving zone located further downstream. If both nozzles operate within a limit cycle, the long term motion dictates that the net energy exchange must be zero. For the Aerodynamic nozzle, a spatial integration of Figure 9 reveals a net driving of 9.1 Joules. This surplus energy is conceivably lost by a variety of mechanisms: viscous dissipation in the boundary layers, non-ideal end reflections, heat lost to the walls, etc. For the Bluff-Body nozzle, however, there appears to be a slightly negative Global Rayleigh Index (-0.2 Joules). Examination of Figure 6 shows that the Heat Release profile is not purely sinusoidal, most likely due to the presence of the diffusion pilot (2%) which has tendencies to modestly effect the heat release profile. The double peaked nature seen in Figure 9 is unique and could also conceivably be due to the premixed pilot which is pulsing in phase with the main combustion zone located further downstream. In any event, the clear reduction in acoustic driving experienced by the Bluff-Body nozzle relative to its aerodynamic counterpart is evident for this generic acoustic cycle.

CONCLUSIONS

Examination of the acoustics for two contrasting fuel/air swirler designs has demonstrated the superiority of the bluff-body configuration with small levels of center-line piloting. Improved acoustic stability was achieved through increased use of the recirculation zone which anchored the main combustion region and reduced the influences of the external flowfield. By liberating the combustion zone from the confines of the recirculation zone, a more favorable acoustic/heat-release coupling is invoked, thereby reinforcing acoustic driving as evidenced by the two-dimensional Rayleigh Indices and finally augmenting oscillatory pressure levels. The contrasting flame stabilization mechanisms have shown marked dissimilarities in two-dimensional driving/damping zones. Improvements to the technique could be made by deconvolution of the axisymmetric image through use of the Abel Transform as done by others (Ref. 23). This represents an important next step in the analysis.

ACKNOWLEDGEMENTS

The authors wish to thank the services of many individuals who aided in the completion of this paper including Miss Luu Vu, Mr. Paul Hamel, Mr. Jason Wegge and Mr. William Proscia.

REFERENCES

1. Leonard, G. and Stegmaier, J., 1994, "Development of an Aeroderivative Gas Turbine Dry Low Emissions Combustion System," *ASME Journal of Engineering for Gas Turbines and Power*, Vol. 116, pp. 542-546.

2. Strand, T., 1996, "Dry Low NOx Combustion Systems Development and Operating Experience," ASME Paper 96-GT-274, Presented at the International Gas Turbine & Aeroengine Congress & Exhibition, June 10-13, Burmingham, United Kingdom.

3. McLeroy, J., Smith, D. and Razdan, M., 1995, "Development and Engine Testing of a Dry Low Emissions Combustor for Allison 501-K Industrial Gas Turbine Engines," ASME Paper 95-GT-335, Presented at the International Gas Turbine & Aeroengine Congress & Exhibition, June 5-8, Houston, TX.

4. Rocha, G., Saadatmand, M. and Bolander, G., 1995, "Development of the Taurus 70 Industrial Gas Turbine," ASME Paper 95-GT-411, Presented at the International Gas Turbine & Aeroengine Congress & Exhibition, June 5-8, Houston, TX.

5. Gysling, D. L., Copeland, G. S., McCormick, D. C., and Proscia, W. M., 1998, "Combustion System Damping Augmentation with Helmholtz Resonators," ASME Paper 98-GT-268, Presented at the International Gas Turbine & Aeroengine Congress & Exhibition, June 2-5, Stockholm, Sweden.

6. Peracchio, A. A. and Proscia, W. M., 1998, "Nonlinear Heat Release/Acoustic Model for Thermoacoustic Instability in Lean Premixed Combustors," ASME Paper 98-GT-269, Presented at the International Gas Turbine & Aeroengine Congress & Exhibition, June 2-5, Stockholm, Sweden.

7. Paschereit, C. O. and Polifke, W., 1998, "Investigation of the Thermoacoustic Characteristics of a Lean Premixed Gas Turbine Burner," ASME Paper 98-GT-582, Presented at the International Gas Turbine & Aeroengine Congress & Exhibition, June 2-5, Stockholm, Sweden.

8. Snyder, T., Rosfjord, T., McVey, J., Hu, A., and Schlein, B., 1994, "Emission and Performance of a Lean-Premixed Gas Fuel Injection System for Aeroderivative Gas Turbine Engines," ASME Paper 94-GT-234, Presented at the International Gas Turbine & Aeroengine Congress & Exhibition, June 13-16, The Hague, Netherlands.

9. Kendrick, D. W., Anderson, T. J., Sowa, W. A., and Snyder, T. S., 1998, "Acoustic Sensitivities of Lean Premixed Fuel Injectors in a Single Nozzle Rig," ASME paper 98-GT-382, Presented at the International Gas Turbine & Aeroengine Congress & Exhibition, June 2-5, Stockholm, Sweden.

10. Anderson, T. J., Sowa, W. A., and Morford, S. A., 1998, "Dynamic Flame Structure in a Low NOx Premixed Combustor," ASME paper 98-GT-568, Presented at the International Gas Turbine & Aeroengine Congress & Exhibition, June 2-5, Stockholm, Sweden.

11. Samaniego, J. M., Egolfopoulos, F. N. and Bowman, C. T., 1995, "CO2* Chemiluminescence in Premixed Flames," *Combustion Science and Technology*, Vol. 109, pp. 183-203.

12. Keller, J. O. and Barr, P. K., 1996, "Premixed Combustion in a Periodic Flow Field," *Unsteady Combustion*, Eds. F. Culick, M. N. Heitor and J. H. Whitelaw, Kluwer Academic, Dordrecht.

13. Raun R. L., Beckstead, M. W., Finlinson, J. C. and Brooks, K. P., 1993, "A Review of Rijke Burners and Related Devices," *Prog. Energy Combust. Sci*., Vol. 19, pp 313-364.

14. Samaniego, J. M., Yip, B., Poinsot, T. and Candel, S., 1993, "Low-Frequency Combustion Instability Mechanism in a Side-Dump Combustor," *Combustion and Flame*, Vol. 94, pp. 163-180.

15. Sterling, J., 1991, "Characterization and Modeling of Aperiodic Pressure Oscillations in Combustion Chambers," AIAA 91-2082, Sacramento, CA.

16. Proscia, W., 1996, Interdepartmental Report on Bulk Mode Instabilities, United Technologies Research Center, E. Hartford, CT.

17. Diederichsen, J. and Gould, R., 1965, "Combustion Instability: Radiation from Premixed Flames of Variable Burning Velocity," Combustion and Flame, Vol. 9, pp. 25-31.

18. Hurle, I., Price, R., Sugden, T. and Thomas, A., 1968, "Sound from Open Turbulent Premixed Flames," *Proc. Roy. Soc.*, Vol. 303, pp. 409-427.

19. Samuelson, R. D., 1967, "Pneumatic Instrumentation Lines and Their Use in Measuring Rocket Nozzle Pressure," NERVA Research and Development Project Report Number RN-DR-0124, Aerojet General Corporation, Sacramento, CA.

20. Kendrick, D. W., 1995, "An Experimental and Numerical Investigation into Reacting Vortex Structures Associated with Pulse Combustion," *Ph.D. Thesis*, Daniel and Florence Guggenheim Jet Propulsion Center, California Institute of Technology, Pasadena, CA.

21. Hedge, U., Reuter, D., Zinn, B., and Daniel, B., 1997, "Fluid Mechanically Coupled Combustion Instabilities in Ramjet Combustors," AIAA paper 87-0216.

22. Barr, P. and Dwyer, H., 1991, "Pulse Combustion Dynamics: A Numerical Study," *Prog. Astro. And Aero*., **135**, pp.673-710.

23. Herding, G., Snyder, R., Rolon, C., and Candel, S., 1998, "Analysis of Flame Patterns in Cryogenic Propellant Combustion," *Journal of Propulsion and Power*, **14**, pp. 146-151.